Mixtures of room temperature ionic liquid/ethanol solutions as electrolytic media for cerium oxide thin layer electrodeposition

Virginie Lair, J. Sirieix-Plenet, L. Gaillon, C. Rizzi, A. Ringuedé

Mixtures of Room Temperature Ionic Liquid/Ethanol Solutions as Electrolytic Media for Cerium Oxide Thin Layer Electrodeposition

V. Lair[*],[a] J. Sirieix-Plenet,[b] L. Gaillon,[b] C. Rizzi,[b] A. Ringuedé[a]

[a] *Laboratoire d'Electrochimie, Chimie des Interfaces et Modélisation pour l'Énergie, LECIME, CNRS UMR 7575-Chimie Paristech (ENSCP)-Paris, 11, rue Pierre et Marie Curie, 75231 Paris cedex 05, France*

[b] *UPMC Univ. Paris 06, UMR 7195, Laboratoire de Physicochimie des Electrolytes, Colloïdes et Sciences Analytiques (PECSA), F-75005 Paris, France ; CNRS, UMR 7195 PECSA, F-75005 Paris, France; ESPCI, UMR 7195, PECSA, F-75005 Paris, France*

CORRESPONDING AUTHOR FOOTNOTE

Tel.: +33155426390. Fax: +33144276750. E-mail: virginie-lair@chimie-paristech.fr

Abstract

A cerium oxide thin layer was electrodeposited onto stainless steel, using mixed room temperature ionic liquid (the 1-methyl-3-butylimidazolium bis(trifluoromethyl sulfonyl)imide)/ethanol solutions, as electrolytic medium. The hydrophobic ionic liquid content is one of the main parameter in the morphology control influencing the ceria growth rate and crystallinity. Micro-nano structural properties and electrical behaviour are presented, using XRD, SEM/EDS and impedance spectroscopy, as a function of electrodeposition conditions.

Keywords Ceria, RTIL, Thin film, Cathodic electrodeposition, Impedance spectroscopy

1. Introduction

Ceria (CeO_2) is a promising material for the surface treatment of different metals and alloys, because of its corrosion resistance in aggressive media [1-4]. Because inorganic crystals chemical reactivity, electronic structure, bonding, and surface energy are directly related to their surface morphology, the ability to tune their shape is a challenging research [5]. It is generally achieved by a precise control of the growth conditions, for a given composition of the solutions or by using surfactants [6-10].

Among the different techniques, such as radiofrequency magnetron sputtering [11], laser beam evaporation ion [12], chemical vapour deposition [13,14] sol-gel processing [15,16], spray pyrolysis [17], or immersion [18-22], that have been used to obtain cerium oxide films, electrodeposition is an attractive method. Cerium oxide films have been obtained by cathodic [23-30] or anodic [31-33] deposition on different substrates and in various solvents [24].

Electrodeposition offers, on one hand, the advantage of controlled thickness of the film, low processing temperature, and high purity and, on the other hand, is a low cost process. It also has been shown to be well-suited for growing thin films composed of crystals with controllable morphology [34]. A unique feature of this method is the ability to tune the orientation, morphology, and chirality of electrodeposited films by monitoring the composition of the electrochemical solution, adding for example complexing agents, or dyes [35-39].

Room temperature ionic liquids (RTILs) have drawn a great interest in recent years because of their attractive chemical and physical properties, such as high chemical and thermal stability, negligible vapor pressure, high conductivity, wide electrochemical window, and the ability to dissolve a large variety of organic and inorganic compounds. They have been used in various fields including organic and inorganic synthesis, catalysis, and electrochemistry [40]. Electrodeposition of nanocrystalline metals and semiconductors is of fundamental interest and finds never ending developments as testifies the growing number of studies reported in recent reviews [41,42]. But so far, very few works were

devoted to the effect of addition of RTILs for inorganic material synthesis, especially for electrodeposited metal oxide thin films.

Generally metal oxide films are obtained by post treatment of the ionic liquid electrodeposited metal film [43,44] or by anodisation of metallic electrodes [45]. Apart from these methods, it is worth to mention that Cu_2O crystals, that could previously be obtained solely by control of the pH solution [36,37] or use of organic additives [38] in aqueous media were synthesized in an ionic liquid/water mixture with tunable morphology [46]. In this mixture, the hydrophilic ionic liquid cations were supposed to slow the growth rates in defined directions.

Until now, to our knowledge, only Azaceta *et al.* [47] described the use of molecular oxygen and ionic liquids to obtain electrodeposited thin films. ZnO nanocrystalline layers were electrodeposited by reaction of Zn^{2+} and superoxide ions generated from the O_2 reduction. In this case, grains and agglomerates growths were also affected by the ionic liquid media in a different mechanism than in conventional aqueous synthesis.

This paper deals with the cathodic electrodeposition and characterisation of cerium oxide films by molecular oxygen activation onto stainless steel substrates via Ce(III) nitrate in pure ionic liquid and in ionic liquid/ethanol mixtures solutions. These new electrolytic compositions, from diluted ionic liquid up to pure hydrophobic IL ($BMImNTf_2$), allow smooth and adherent cerium oxide thin films to be obtained. The deposited oxide films are composed of small particles of cerium oxide lying on a dense and compact amorphous phase.

2. Experimental

2.1. Chemicals

Cerium nitrate ($Ce(NO_3)_3,6H_2O$), Alfa Aesar, 99.5%), absolute ethanol (99.8 %, Carlo Erba ACS-for

analysis), dichloromethane (stabilized with *ca.* 100 ppm amylene, ACROS Organics ACS-for analysis), 1-methylimidazole (ACROS Organics), $LiNTf_2$ (> 99 %, Fluka) were used without additional purification.

The ionic liquid $BMImNTf_2$ was prepared by reaction of 1-methylimidazole and 1-bromobutane followed by metathesis with $LiNTf_2$ in water [48]. The resulting product was extracted with dichloromethane and washed several times with water until the $AgNO_3$ test, which allows one to trace even very low contents of halide-based impurities, became negative. Then, dichloromethane phase was dried ($MgSO_4$) and evaporated. The residue was lyophilized and was kept under argon.

The final product was characterized by ^1H NMR (200 MHz, $CDCl_3$) δ (ppm): 1.0 (t, ^3J= 7.3 Hz, $C\underline{H_3}CH_2$); 1.4 (m, $CH_3C\underline{H_2}CH_2$); 1.9 (m, $C\underline{H_2}CH_2N$); 4.0 (s, $C\underline{H_3}N$); 4.2 (t, ^3J= 7.4 Hz, $C\underline{H_2}N$); 7.3 (m, H_{Im}); 8.8 (s, H_2), and by mass spectrometry using Electrospray (ESI) positive mode m/z = 138.9 $[M\text{-}NTf_2]^+$, 558.0 $(2M\text{-}NTf_2)^+$, and negative mode m/z = 279.8 $[M\text{-}BMIm]^-$ where M is $BMImNTf_2$.

The water content value in $BMImNTf_2$ was determined by using standard Karl-Fischer method (coulometric titrator titroline KF trace, Schott instruments) and was equal to 130 ppm.

2.2. Electrochemical measurements

A classical 3-electrodes cell was used for all electrochemical experiments. The counter electrode was a platinum wire whereas the reference electrode was a saturated calomel electrode (E(SCE) = 0.24 V/SHE). This reference electrode was protected from diffusion by a capillary filled with agar-agar gel. In addition to the three electrodes, the electrochemical cell contained gas inlet and outlet.

Ceria thin films were deposited on a stainless steel foil (316L from Goodfellow) with a 2 cm^2 surface. All the deposits were realized at room temperature, under stirring and oxygen bubbling. A potentiostatic method was used, in which a reductive potential between -1.4V and -0.6 V/SCE was applied for 2h. The

chronoamperograms were obtained using a Biologic potentiostat and its EC lab express software.

The study of the electrochemical window of the electrolyte was classically done under argon bubbling. Different mixtures of $BMImNTf_2$ and ethanol were used (Table 1) as electrolyte, all of them containing 5 10^{-2} mol kg^{-1} of cerium (III) nitrate. Ethanol can be mixed in all proportions with this ionic liquid known as hydrophobic, and the cerium salt was easily solubilised in every electrolyte studied.

2.3. Morphological, structural and electrical characterizations

The ceria films were characterized by X-ray diffraction (XRD) measurements, using a Philips PW 1390 diffractometer with the Co K_α radiation (1.78897 Å) and 2θ varying from 15 to 70°. The diffraction pattern was scanned by steps of 0.02° with 2 s counting times.

The microstructures of the deposited films were studied using a field emission scanning electron microscope (FEG-SEM, Zeiss system model Ultra 55, resolution 1 nm) coupled to EDS (detector SDD X-FLASH 4010 Bruker, resolution 123 eV).

The electrical resistance of the deposit was determined by impedance spectroscopy measurements, using a PGSTAT 30 model potentiostat, Autolab Ecochemie BV. The signal amplitude was fixed at 100 mV with respect to the system linearity, within the 1 MHz to 10 mHz frequency range, using 11 points per decade. Measurements were carried out as a function of temperature, under ambient atmospheric air. A specific configuration to study the electrical behavior of the thin layers was considered, *i.e.* a dissymmetric two electrodes configuration: the working electrode is a platinum pointed electrode, while a platinum spiral, used as current collector, was in contact on the other side with the stainless steel conductive substrate (counter-electrode and reference electrode were finally short-circuited) [49].

3. Results and discussion

3.1. Electrochemical studies

The electroactive windows were first determined for each electrolyte, under argon bubbling. Cyclic voltammograms obtained for all electrolytes are shown in Figure 1. For electrolytes that contained a quite huge amount of ethanol (M_1, M_2, M_3, M_4), the reduction limit appeared at about -1V/SCE (-1.0V for M_4, -1.1V for M_3 and -1.2V for both M_2 and M_1). The reductive limit seemed to vary slightly towards more positive potentials with an increasing amount of RTIL. Nevertheless, for the pure ionic liquid (M_p) , the behavior was totally different and did not follow the tendency. Indeed, the limit appeared farther at about -1.8V/SCE since the $BMImNTf_2$ is well known for its large electrochemical domain of stability. No additional peak appeared indicating that every electrolyte was stable in the reductive window up to the reductive limit, with no trace of any impurities.

In order to determine the working potential for electrodeposition, cyclic voltammograms under oxygen bubbling were recorded in the same domain of potentials. The response obtained in electrolyte M_3 is shown in Figure 2. A reductive wave appeared at half potential close to - 0.8V/SCE and a minimum peak at about -1V/SCE due to the reduction of dissolved O_2. The voltammogram observed for all other electrolyte compositions displayed the same pattern (data not shown).

The peak potentials of the reductive peak for each electrolyte are summed up in Table 2. The reductive wave appeared in each electrolyte, at quite the same potential except for M_p. The oxygen reduction wave was shifted in pure IL towards the more reductive potentials. This shift of peak potential toward more negative value was observed as solvating properties of the solvent toward oxygen were modified.

These results are in good agreements with results already published for molecular oxygen

electrochemical studies in $BMImNTf_2$ [50-53] as well as in other ionic liquids [54-63]. Solubility of O_2 [50],[54],[58],[62] and reversibility of its reduction have been thoroughly studied in RTIL. The stability of the electrogenerated superoxide $O_2^{\cdot -}$ is related to ions interactions between the radical anion and the ionic liquid cations [54].

3.2. Electrodeposition of ceria

The electrodeposition was carried out applying a fixed potential closed to the reduction peak potential (see Table 2). The chronoamperograms obtained for each electrolyte are shown in Figure 3. The curves presented noisy background due to the stirring, which let the working electrode move slightly.

The general shape was comparable for each electrolyte (M_1 to M_4). The current rapidly decreased in the first 1000 s and then seemed to reach a plateau. The more the RTIL in the electrolyte composition, the larger the current of the plateau. All the deposits were dark yellow and appeared quite homogeneous. The case of pure IL was quite different from the others. The current didn't decrease but it stayed constant during all the deposition time. That could suggest that no deposition occurs which is confirmed by the absence of visible deposit on the stainless steel foil.

A slight decrease of the current was sometimes due to a non constant O_2 bubbling for a few seconds. The chronoamperogram for the electrolyte M_4 was less smooth than the other. For this high fraction of RTIL, the increased viscosity of the mixture affected the oxygen supply to the solution.

3.3. Morphological, structural and electrical characterisations

To ensure the formation of cerium-based films, XRD patterns have been plotted, as shown in **Figures 4 (a) and 4 (b)**. X-ray diffraction patterns indicated that cathodic deposits obtained from the mixed RTIL/ethanol solutions (M_1 to M_4) exhibited one main broad peak attributed to (111) planes of the ceria phase when crystallised in a cubic symmetry (JCPDS file #43 -1002). The width of the peaks indicated

that the deposit was not fully crystallised. Comparing the XRD patterns for the four electrolytes, it was obvious that the thickness of the ceria-based layer in mixed RTIL/ethanol solutions depended on the amount of RTIL: the more $BMImNTf_2$, the thicker the layer. Because of the higher viscosity of the pure $BMImNTf_2$ solution, the ceria deposit growth was slower in this media.

After heat treatment at a relatively low temperature (400°C), the crystallinity of the obtained deposit was obviously improved, as shown from the electrolyte M_3 in **Figure 4 (b)**. All the more intense peaks corresponding to the usual cubic ceria phase were present and well-defined. The crystallite size, even if slightly higher (4.6 nm) than in the as-deposited films, remained close to it. This better definition of the cubic phase of the ceria film could be the result of a loss of organic compounds due to the decomposition of element coming from the $BMImNTf_2$ used. It was already observed that entrapment of RTIL during electrodeposition could occur, and correlated to a loss of mass during thermal analysis [64].

SEM investigation of the surface of CeO_2 thin film showed that depending on the RTIL/ Ethanol composition, we could observe either dense or mixed porous/dense morphology of the deposit. For example, for M_3 (see **Figure 5 (a)**), we observed that the stainless steel was covered but the film was cracked. No noticeable difference was observed by SEM after heat treatment (data not shown). The morphology and structure of this film are shown in **Figure 5 (b).** It could be assessed that the film was built up of a dense and compact thin film of about 1.9 µm thickness exhibiting dispersed spherical agglomerates on the top. This upper layer seemed to be more porous and was about 3.5 µm thick. Thickness was deduced from SEM analysis of a side view of the deposit tilted with a known angle. Values are given after angle correction.

As the thin film could find applications for high temperature devices such as fuel cell, it was relevant to study the type of conductivity, ionic or electronic, it presented. Accordingly, impedance spectroscopy measurements were carried out as a function of the temperature, under air atmospheric pressure. **Figure**

6 gives a typical Nyquist diagram obtained on ceria deposit, as fabricated in M_3. One can separate two main contributions, depending on the signal amplitude variation. At high frequencies, up to 1 kHz in that case, one main semi-circle was defined, ascribed to the ionic behaviour of the oxide layer as already demonstrated [49]. The lowest frequency range, *i.e.* from 1 kHz to 1 Hz in this diagram, corresponded to the interfacial phenomena and substrate behaviour (stainless steel). Full decomposition and analysis are currently in progress. To confirm the ionic contribution of the oxide layer, the resistance of this contribution was reported in an Arrhenius plot (Figure 7), as a function of the reverse temperature.

Linear plot was observed even for temperature as low as 300°C. The activation energy of 1.2eV, deduced from the slope of this plot, is typical of a largely dominant ionic conductivity when oxide ion conductors are of concern.

It could however be noticed that this activation energy was slightly higher than the one observed for sintered materials, more often close to 0.9 eV, as already observed [28]. From the relaxation frequency of the high frequency contribution, a dielectric constant equal to 2 was calculated. As reported in literature, such value was characteristic of ceria, for bulk [65], even when deposited in aqueous media [28].

In water, the mechanism generally postulated for the electrodeposition of ceria, implies the precipitation of Ce(IV) with hydroxides, the latter coming from the electrochemical reduction of molecular oxygen. In our media, unavoidable water traces could allow synthesizing hydroxide ions via a similar mechanism, as we showed that previous O_2 reduction was required for ceria deposition in $BMImNTf_2$/ethanol mixtures. In a recent published article [66], cathodic deposition of cerium oxides was investigated in ethanol. In presence of oxygen, another mechanism was postulated involving the formation of an electrogenerated peroxide resulting from oxygen reduction. The authors suggested the possibility that a positively charged complex between Ce^{3+} and peroxide first formed which could then be reduced as Ce_2O_3. More experiments would be required to find out which species is more likely to

participate in the mechanism involved in RTIL/ethanol mixtures.

4. Conclusions

CeO_2 thin films were electrodeposited on stainless steel, used as the cathode, from mixtures containing the hydrophobic RTIL, $BMImNTf_2$, and ethanol. The films obtained were homogeneous and adherent and their thickness correlated well with the RTIL content of the electrolyte.

The X-ray diffraction confirmed the formation of cubic phase ceria and indicated that the crystallinity could be improved after thermal treatment. Microscopic observations revealed that the ceria films surface displayed some cracks and that it was typically composed of a dense layer covered by a thicker porous layer made of dispersed clusters. The ionic conductivity of the films was confirmed.

The RTILs / ethanol mixtures seem to be a promising new class of solvents for the morphology control of electrodeposited materials. The influence of the ionic liquid in mixture with ethanol as well as deposition parameters such as applied cathodic current density, deposition time and composition of the bath are under investigation. Experiments are currently performed in other RTIL/organic solvents mixtures and first results are quite promising.

Acknowledgment

This work is supported by ANR (Agence Nationale de la Recherche – France), ANR JCJC06-0131 COMICEL program.

The SEM and EDX analyses were made by S. Borensztajn from the laboratory LISE in Paris, France.

References

[1] B. R. W. Hinton, J. Alloys Compd. 180 (1992) 15.

[2] R. Thanneeru, S. Patil, S. Deshpande, S. Seal, Acta Mater. 55 (2007) 3457.

[3] R. Liu, D. Y. Li, J. Mater. Sci. 35 (2000) 633.

[4] E. Stoyanova, D. Guergova, D. Stoychev, I. Avramova, P. Stefanov, Electrochim. Acta 55 (2010) 1725.

[5] Q. Yuan, H.-H. Duan, L.-L. Li, L.-D. Sun, Y.-W. Zhang, C.-H. Yan, J. Colloid Interface Sci. 335 (2009) 151.

[6] V. F. Puntes, K. M. Krishnan, A. P. Alivisatos, Science 291 (2001) 2115.

[7] Y. Sun, Y. Xia, Science 298 (2002) 2176.

[8] L. F. Gou, C. J. Murphy, Nano Lett. 3 (2003) 231.

[9] S. Mann, Angew. Chem. Int. Ed. 39 (2000) 3393.

[10] C. H. Lu, L. M. Qi, J. H. Yang, X. Y. Wang, D. Y. Zhang, J. L. Xie, J. M. Ma, Adv. Mater. 17 (2005) 2562.

[11] M. Vaclavu, I. Matolinova, J. Myslivecek, R. Fiala, V. Matolin, J. Electrochem. Soc. 156 (2009) B938.

[12] S. Kanakaraju, S. Mohan, A. K. Sood, Thin Solid Films 305 (1997) 191.

[13] J. F. Jue, J. Jusko, A. V. Virkar, J. Electrochem. Soc. 139 (1992) 2458.

[14] M. J. Capitan, A. Paul, J. L. Pastol, J. A. Odriozola, Oxid. Met. 52 (1999) 447.

[15] N. Ozer, Sol. Energy Mater. Sol. Cells 68 (2001) 391.

[16] C. Agrafiotis, A. Tsetsekou, C. J. Stournaras, A. Julbe, L. Dalmazio, C. Guizard, J. Colloid. Surf. sci. 22 (2002) 15.

[17] K. Konstantinov, I. Stambolova, P. Peshev, B. Darriet, S. Vassilev, Int . J. Inorg. Mat. 2 (2000) 277.

[18] A. J. Davenport, H. S. Isaacs, M. W. Kendig, Corros. Sci. 32 (1991) 653.

[19] W. G. Fahrenholtz, M. J. O'Keefe, H. F. Zhou, J. T. Grant, Surf. Coat. Technol. 155 (2002) 208.

[20] M. G. S. Ferreira, R. G. Duarte, M. F. Montemor, A. M. P. Simoes, Electrochim. Acta 49 (2004) 2927.

[21] M. A. Arenas, J. J. de Damborenea, Surf. Coat. Technol. 187 (2004) 320.

[22] K. Aramaki, Corros. Sci. 46 (2004) 1565.

[23] L. Arurault, P. Monsang, J. Salley, R. S. Bes, Thin Solid Films 466 (2004) 75.

[24] P. Stefanov, G. Atanasova, D. Stoychev, T. Marinova, Surf. Coat. Technol. 180-81 (2004) 446.

[25] Y. C. Zhou, J. A. Switzer, J. Alloys Compd. 237 (1996) 1.

[26] I. Zhitomirsky, A. Petric, Ceram. Int. 27 (2001) 149.

[27] F. B. Li, G. E. Thompson, J. Electrochem. Soc. 146 (1999) 1809.

[28] V. Lair, A. Ringuedé, P. Vermaut, S. Griveau, Phys. Stat. Sol. C 5 (2008) 3492.

[29] Y. Hamlaoui, F. Pedraza, C. Remazeilles, S. Cohendoz, C. Rebere, L. Tifouti, J. Creus, Mater. Chem. Phys. 113 (2009) 650.

[30] H. Elbelghiti, V. Lair, A. Ringuedé, M. Cassir, ECS Trans. 7 (2007) 2391.

[31] M. Balasubramanian, C. A. Melendres, A. N. Mansour, Thin Solid Films 347 (1999) 178.

[32] A. Q. Wang, T. D. Golden, J. Electrochem. Soc. 150 (2003) C616.

[33] T. D. Golden, A. Q. Wang, J. Electrochem. Soc. 150 (2003) C621.

[34] G. Hodes, Electrochemistry of Nanomaterials, New York, 2001.

[35] J. A. Switzer, H. M. Kothari, P. Poizot, S. Nakanishi, E. W. Bohannan, Nature 425 (2003) 490.

[36] R. Liu, F. Oba, E. W. Bohannan, F. Ernst, J. A. Switzer, Chem. Mater. 15 (2003) 4882.

[37] J. A. Switzer, H. M. Kothari, E. W. Bohannan, J. Phys. Chem. B 106 (2002) 4027.

[38] M. J. Siegfried, K. S. Choi, Angew. Chem. Int. Ed. 44 (2005) 3218.

[39] T. Yoshida, H. Minoura, Adv. Mater. 12 (2000) 1219.

[40] H. Ohno, Electrochemical aspects of ionic liquids, New York, 2005.

[41] F. Endres, D. MacFarlane, A. Abbott, Electrodeposition from Ionic Liquids, New York, 2008.

[42] W. Simka, D. Puszczyk, G. Nawrat, Electrochim. Acta 54 (2009) 5307.

[43] J.-K. Chang, C.-H. Huang, W.-T. Tsai, I.-W. Sun, P.-Y. Chen, ECS Trans. 6 (2008) 165.

[44] C. Arnould, J. Delhalle, Z. Mekhalif, Electrochim. Acta 53 (2008) 5632.

[45] N. Liu, D. Wu, H. X. Wu, F. Luo, J. Chen, Solid State Sci. 10 (2008) 1049.

[46] H. Li, R. Liu, R. Zhao, Y. Zheng, W. Chen, Z. Xu, Crystal Growth & Design 6 (2006) 2795.

[47] E. Azaceta, R. Tena-Zaera, R. Marcilla, S. Fantini, J. Echeberria, J. A. Pomposo, H. Grande, D. Mecerreyes, Electrochem. Comm. 11 (2009) 2184.

[48] P. Bonhote, A. P. Dias, N. Papageorgiou, K. Kalyanasundaram, M. Gratzel, Inorg. Chem. 35 (1996) 1168.

[49] C. Brahim, F. Chauveau, A. Ringuedé, M. Cassir, M. Putkonen, L. Niinisto, J. Mater. Chem. 19 (2009) 760.

[50] X. J. Huang, E. I. Rogers, C. Hardacre, R. G. Compton, J. Phys. Chem. B 113 (2009) 8953.

[51] A. Rene, D. Hauchard, C. Lagrost, P. Hapiot, J. Phys. Chem. B 113 (2009) 2826.

[52] J. Ghilane, C. Lagrost, P. Hapiot, Anal. Chem. 79 (2007) 7383.

[53] A. Noda, A. B. Susan, K. Kudo, S. Mitsushima, K. Hayamizu, M. Watanabe, J. Phys. Chem. B 107 (2003) 4024.

[54] A. S. Barnes, E. I. Rogers, I. Streeter, L. Aldous, C. Hardacre, G. G. Wildgoose, R. G. Compton, J. Phys. Chem. C 112 (2008) 13709.

[55] M. C. Buzzeo, O. V. Klymenko, J. D. Wadhawan, C. Hardacre, K. R. Seddon, R. G. Compton, J. Phys. Chem. A 107 (2003) 8872.

[56] I. M. AlNashef, M. L. Leonard, M. C. Kittle, M. A. Mattews, J. W. Weidner, Ind. Eng. Chem. Res. 482 (2002) 87.

[57] D. Zhang, T. Okajima, F. Matsumoto, T. Ohsaka, J. Electrochem. Soc. 151 (2004) D31.

[58] Y. Katayama, K. Sekiguchi, M. Yamagata, T. Miura, J. Electrochem. Soc. 152 (2005) E247.

[59] M. M. Islam, T. Ohsaka, J. Phys. Chem. C 112 (2008) 1269.

[60] D. Zigah, A. F. Wang, C. Lagrost, P. Hapiot, J. Phys. Chem. B. 113 (2009) 2019.

[61] R. G. Evans, O. V. Klymenko, S. A. Saddoughi, C. Hardacre, R. G. Compton, J. Phys. Chem. B 108 (2004) 7878.

[62] D. S. Silvester, E. I. Rogers, L. E. Barrosse-Antle, T. L. Broder, R. G. Compton, J. Braz. Chem. Soc. 19 (2009) 611.

[63] L. Gaillon, F. Bedioui, Chem. Commun. (2001) 1458.

[64] P. Giridhar, K. A. Venkatesan, T. G. Srinivasan, P. R. V. Rao, Electrochim. Acta 52 (2007) 3006.

[65] M. Hartmanova, K. Gmucova, I. Thurzo, Solid State Ionics 130 (2000) 105.

[66] I. Valov, D. Guergova, D. Stoychev, NATO Advanced Study Institute, Nanotechnological Basis for Advanced Sensors, Sozopol, Bulgaria, 30 may - 10 june 2010, in press.

Figure 1. Cyclic voltammograms obtained on stainless steel 316L of electrolytes M_1, M_2, M_3, M_4, and M_p saturated with argon at room temperature (scan rate 50 mV s^{-1}, geometric surface area 2 cm^2).

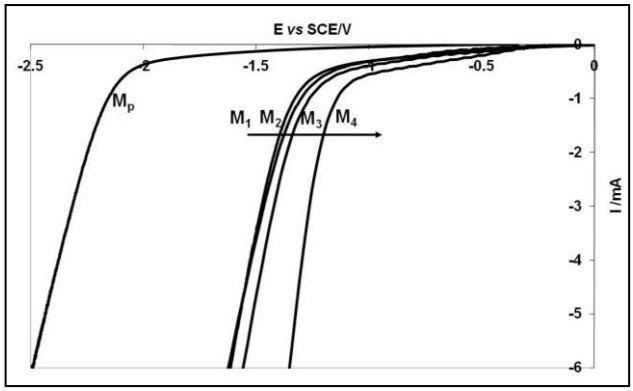

Figure 2. Cyclic voltammograms obtained at room temperature on stainless steel 316L in electrolyte M_3 saturated with argon (a) or oxygen (b) (scan rate 50 mV s^{-1}, geometric surface area 2 cm^2).

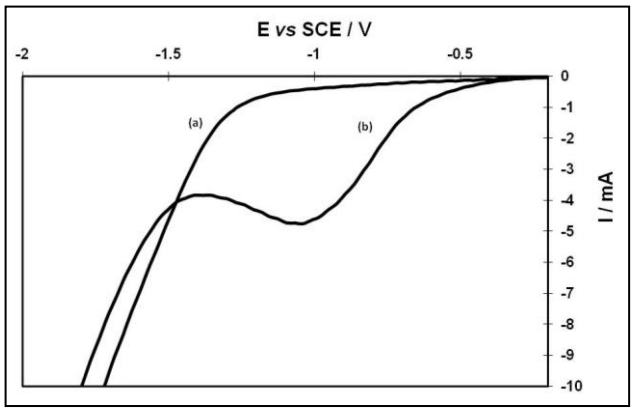

Figure 3. Chronoamperograms obtained at room temperature on stainless steel 316L under oxygen bubbling for the deposition of ceria in electrolytes M_1, M_2, M_3, M_4, and M_p: cerium(III) nitrate 0.05 mol kg^{-1} (geometric surface area 2 cm^2).

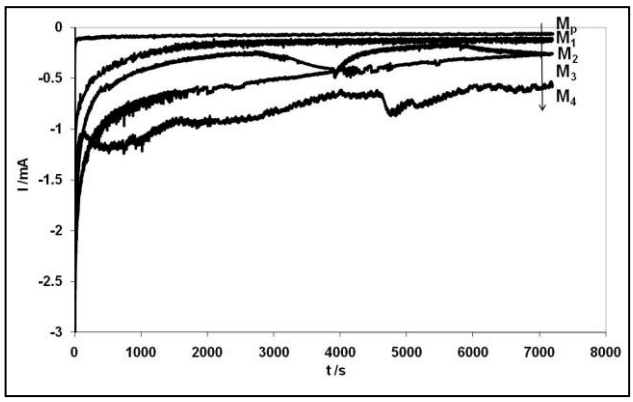

Figure 4. XRD pattern of ceria electrodeposited film (a) in M_1, M_2, M_3, and M_4 as prepared and (b) in M_3 before (curve α) and after (curve β) heat treatment (400°C, 2 hours). * indicates peaks due to the stainless steel substrate. (Co Kα radiation (1.78897Å); 25°<2θ<75°; steps of 0.02°). All the patterns are normalized toward (a) the first peak (111) and (b) the first peak of the substrate.

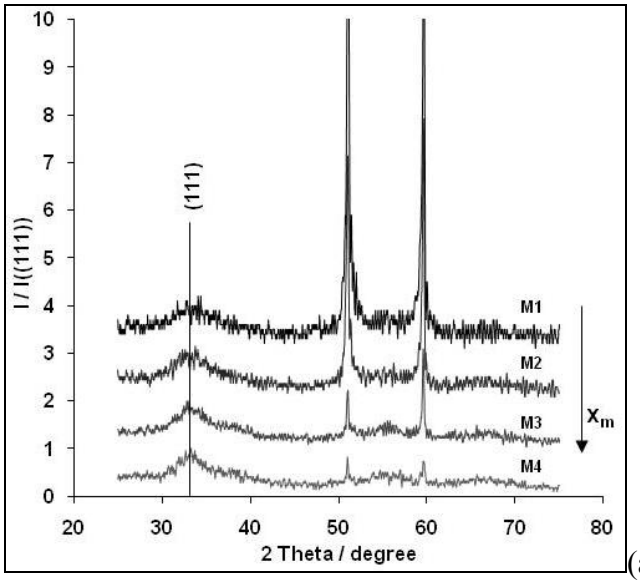

(a)

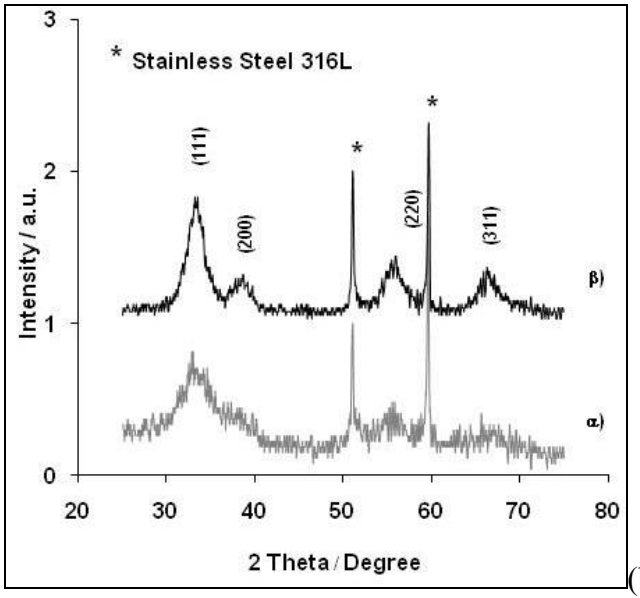

(b)

Figure 5. SEM observations of ceria deposit obtained on stainless steel in electrolyte M_3 (ULTRA 55 ZEISS - 1 nm resolution) (a) film surface (b) cross section (the sample was tilted with an angle of 65°).

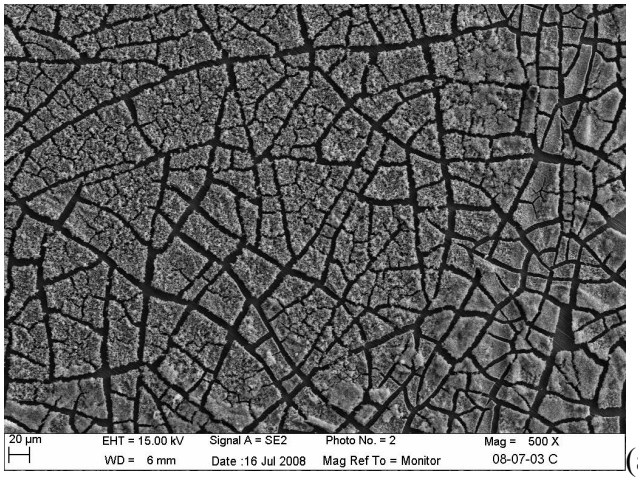

(a)

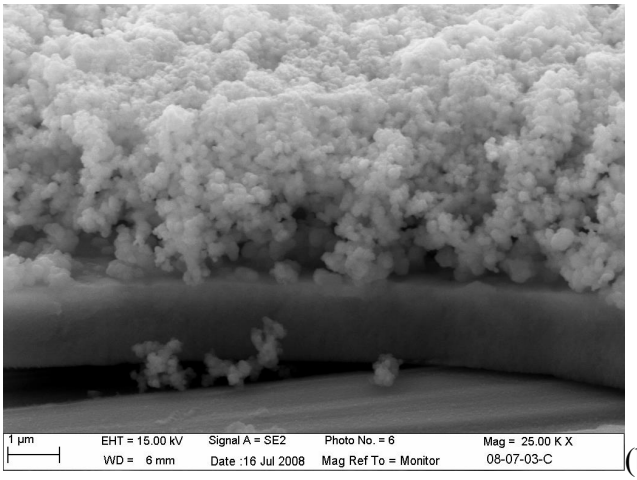

(b)

Figure 6. Impedance diagram measured at 300°C, under air, ΔE = 100 mV. Numbers indicate the logarithm of the signal frequency.

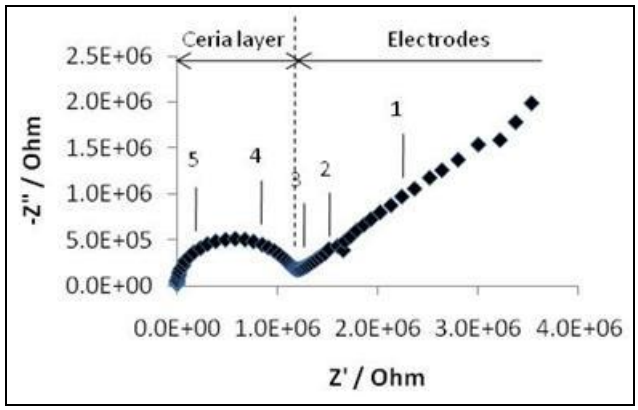

Figure 7. Arrhenius plot of the M_3 layer resistance, deduced from impedance diagrams.

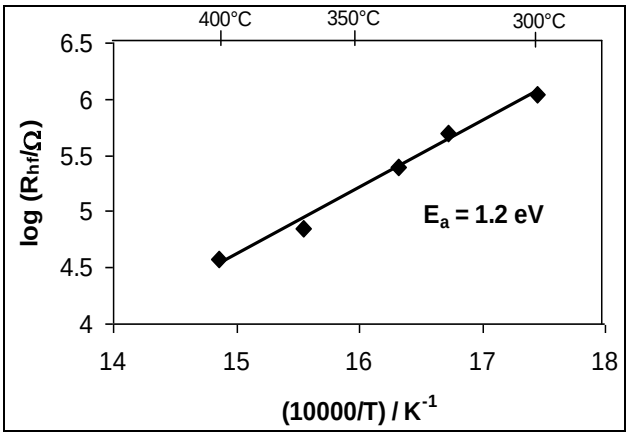

Figures captions

Figure 1. Cyclic voltammograms obtained on stainless steel 316L of electrolytes M_1, M_2, M_3, M_4, and M_p saturated with argon at room temperature (scan rate 50 mV s^{-1}, geometric surface area 2 cm^2).

Figure 2. Cyclic voltammograms obtained at room temperature on stainless steel 316L in electrolyte M_3 saturated with argon (a) or oxygen (b) (scan rate 50 mV s^{-1}, geometric surface area 2 cm^2).

Figure 3. Chronoamperograms obtained at room temperature on stainless steel 316L under oxygen bubbling for the deposition of ceria in electrolytes M_1, M_2, M_3, M_4, and M_p: cerium(III) nitrate 0.05 mol kg^{-1} (geometric surface area 2 cm^2).

Figure 4. XRD pattern of ceria electrodeposited film (a) in M_1, M_2, M_3, and M_4 as prepared and (b) in M_3 before (curve α) and after (curve β) heat treatment (400°C, 2 hours). * indicates peaks due to the stainless steel substrate. (Co Kα radiation (1.78897Å); $25° < 2\theta < 75°$; steps of 0.02°). All the patterns are normalized toward (a) the first peak (111) and (b) the first peak of the substrate.

Figure 5. SEM observations of ceria deposit obtained on stainless steel in electrolyte M3 (Ultra 55 ZEISS – 1nm resolution) (a) film surface (b) cross section (the sample was tilted with an angle of 65°)

Figure 6. Impedance diagram measured at 300°C, under air, ΔE = 100 mV. Numbers indicate the logarithm of the signal frequency.

Figure 7. Arrhenius plot of the M_3 layer resistance, deduced from impedance diagrams.

TABLE 1: Electrolyte M_x where x_{IL} is the mass fraction of $BMImNTf_2$ in its mixture with ethanol.

Electrolyte	M_1	M_2	M_3	M_4	M_p
x_{IL}	0.17	0.44	0.65	0.80	1.00

TABLE 2: Peak potential of O_2 reduction in electrolytes M_1, M_2, M_3, M_4, and M_p.

Electrolyte	M_1	M_2	M_3	M_4	M_p
Peak potential (*vs* SCE/V)	-1.1	-1.1	-1.0	-0.8	-1.6

Tables captions

TABLE 1: Electrolyte M_x where x_{IL} is the mass fraction of $BMImNTf_2$ in its mixture with ethanol.

TABLE 2: Peak potential of O_2 reduction in electrolytes M_1, M_2, M_3, M_4, and M_p.